In-situ alloying of Ti-xPt using laser powder bed fusion to produce novel alloys

Gerrit Ter Haar[1*], *Dean-Paul* Kouprianoff[2]

[1]Mechanical and Mechatronic Engineering Department, Faculty of Engineering, Stellenbosch University, Stellenbosch, South Africa
[2]Centre for Rapid Prototyping and Manufacturing, Central University of Technology, Bloemfontein, South Africa

Abstract. This study investigates the in-situ alloying of Ti-xPt (x = 5, 10 wt%) using laser powder bed fusion (L-PBF) to produce novel alloys with enhanced electrochemical properties. Two different powder mixtures and process parameter sets were employed to evaluate the influence of composition and processing conditions on microstructure development and electrochemical performance. The samples with 5 wt% Pt achieved full density, while the ones with 10 wt% Pt exhibited approximately 91% relative density due to incomplete fusion at Ti-Pt interfaces. Microstructural analysis revealed the formation of Ti3Pt and Ti2Pt intermetallic compounds at the partially alloyed interfaces, with significant Pt diffusion evidenced by increased hardness values compared to cp-Ti. Electrochemical testing demonstrated superior corrosion resistance in all samples of Ti-xPt, with corrosion potentials shifting positively from -304.5 mV for cp-Ti to between -10.9 and -23.3 mV. Notably, the hydrogen evolution reaction performance of the Ti-xPt alloys matched or exceeded that of pure platinum, with most samples requiring lower over-potentials at 10 mA/cm². These findings demonstrate that L-PBF-processed Ti-Pt alloys with minimal platinum content can achieve excellent electrochemical properties, presenting significant cost advantages for biomedical and energy conversion applications where platinum's catalytic properties are essential.

1 Introduction

Titanium-platinum (Ti-Pt) alloys represent a promising class of materials that combine exceptional mechanical properties with superior electrochemical properties, making them ideal candidates for demanding applications in biomedical, aerospace, and energy conversion industries. While their potential has been recognized in literature, the manufacturing challenges associated with these intermetallic compounds have limited their practical implementation and comprehensive characterization [1] The advent of additive manufacturing, particularly Laser Powder Bed Fusion (L-PBF), offers new possibilities for processing these complex alloy systems through in-situ alloying. This technique not only addresses manufacturing limitations but also provides a novel approach to investigate previously unexplored material properties, phases, and microstructures in the Ti-Pt system.

* Corresponding author: gterhaar@sun.ac.za

The inclusion of platinum is particularly significant given its critical role as a catalyst in water electrolysis processes, where its unique electronic structure facilitates efficient hydrogen evolution reactions [2].

In biomedical applications, concerns regarding the cytotoxicity of conventional Ti-6Al-4V alloys have spurred research into safer alternatives incorporating non-toxic elements like Pt. Even small additions of platinum to titanium substantially enhance corrosion resistance through improved active-passive transitions, with studies confirming significantly reduced ion release from Ti-Pt alloys containing as little as 0.5 wt% Pt compared to conventional titanium materials [3]. For energy conversion applications, particularly water electrolysis, platinum's exceptional catalytic properties make it invaluable. As a cathode catalyst, Pt exhibits optimal hydrogen intermediate binding strength—the "Goldilocks" property that minimizes overpotential and enables efficient hydrogen evolution at lower applied voltages [4]. Despite ongoing research into alternatives driven by platinum's scarcity and cost, its unmatched activity, acidic stability, and operational longevity remain the gold standard for industrial electrolysis systems [5].

Traditional manufacturing methods for Ti-Pt alloys present several limitations, including high material costs, challenges in achieving precise compositional control, and difficulties in fabricating complex geometries [1]. Furthermore, conventional processing routes often struggle to produce the unique microstructures that might optimize the performance of these alloys in terms of corrosion resistance and catalytic activity for electrochemical applications. These limitations have restricted both fundamental research into the Ti-Pt system and its practical applications.

L-PBF has emerged as a breakthrough technology that offers unique advantages for processing metallic materials. For the Ti-Pt system specifically, L-PBF presents several compelling opportunities: (1) the ability to create complex geometries essential for biomedical implants and aerospace components; (2) potential for precise compositional control through in-situ alloying; (3) significant cost reduction through material efficiency, particularly important when working with precious metals like platinum; and (4) the possibility of achieving unique non-equilibrium microstructures that may exhibit enhanced properties [6].

While L-PBF of pure Pt has gained traction in the jewellery industry, and some studies have investigated Ti alloys with Pt content up to 20 wt% [7], to the authors' knowledge, no comprehensive study has investigated the in-situ alloying of Ti-Pt or published detailed characterization of Ti-Pt phases and microstructures at varying Pt content produced via L-PBF . This presents both a knowledge gap and a research opportunity, as in-situ alloying through LPBF could serve not only as a manufacturing method but also as a novel approach to investigate new phases in the Ti-Pt system.

The present study aims to address this gap by investigating the in-situ alloying of Ti-xPt (where x = 5 and 10 wt%) through LPBF. Two different powder mixtures and two different processing parameter sets (high and low energy density) were employed to evaluate the influence of composition and processing conditions on microstructure development. While complete homogenization through *in-situ* alloying presents challenges, this work demonstrates that the approach can produce fully dense parts with complex microstructures featuring partially mixed Ti-Pt interfaces. These interfaces provide valuable insights into the phases that form at the Ti-Pt boundary, contributing novel understanding to the Ti-Pt phase diagram.

This research contributes to the field in three significant ways: (1) it establishes the feasibility of using L-PBF for processing Ti-Pt alloys; (2) it provides detailed characterization of the microstructures and phases that develop during in-situ alloying; and (3) it evaluates the relationship between processing parameters, resulting microstructures, and electrochemical behaviour. The findings not only advance our understanding of the Ti-Pt system but also demonstrate the potential of L-PBF as both a manufacturing method for these high-value alloys and as an investigative tool for exploring complex intermetallic systems.

2 Methodology

2.1 Preparation of materials

Two titanium and platinum powder mixtures were prepared by mixing in weight ratios of 5% Pt and 10% Pt. Virgin commercially pure (cp-Ti) powder was acquired from *TLS Technik GmbH & Co.* Lot 1951/3 with a particle size of < 45um was used. Pt powder from batch labelled "inspec 199 8 782" was used for all experiments.

Powder preparation and mixing: Both powders were first dried at 80°C for 2 hours to remove moisture. The powders were then mechanically mixed using a Turbula three-dimensional dynamic mixer for 15 minutes at the University of the Free State to ensure homogeneous distribution of the Pt particles within the Ti matrix powder.

L-PBF procession: A *OR-Laser* L-PBF machine at the Central University of Technology's Centre for Rapid Prototyping and Manufacturing was used to fabricate the samples. Two different parameter sets, tabulated in Table 1, were used. These parameter sets were chosen since they have previously been optimised to achieve high-dense Ti-6Al-4V builds [8]. Therefore, they were selected as a starting point for the Ti-Pt mixed powders. The listed parameters are, P - power, D - laser spot diameter, V - scan speed, H - hatch distance, L - layer thickness, E_v - volumetric laser energy density (calculated as $\frac{P}{V \times H \times L}$), and $\frac{P}{V}$ - linear energy density.

Rectangular plate samples were manufactured with dimensions of 12×1×10 mm (X × Y × Z – with reference to the build plate with Z-axis being perpendicular to the build plate surface and represents the build direction).

Table 1. Process parameter used in parameters sets A and B.

	P [W]	**D [µm]**	**V [mm/s]**	**H [µm]**	**L [µm]**	**E_v [j/mm^3]**	**P/V [j/mm]**
Parameter set A	180	40	1100	115	30	47.43	0.164
Parameter set B	100	75	600	85	30	65.36	0.167

2.2 Sample preparation

After fabrication, samples were prepared for analysis by applying the following sequential sample preparation steps:

1. **Grinding:** Samples underwent sequential grinding using SiC paper starting with 320 grit, followed by 800 grit to remove surface roughness and build artifacts.

2. **Polishing:** This was followed by polishing using 9 µm diamond suspension with 5 N force for 5 minutes. Subsequently, 0.25 µm (OP-S) suspension was applied for 4 minutes using 25 N load, and the process was completed with 0.04 µm (OP-U) for 4 minutes at 25 N load to achieve a mirror-like finish.
3. **Cleaning:** Samples were cleaned in isopropanol between each step and at the end of the preparation process to remove polishing residues.
4. **Etching:** Chemical etching was performed by submerging samples in a water-based solution containing 2.2 wt% HF and 20 wt% HNO_3 for 20-30 seconds to reveal microstructural features.
5. **Final cleaning:** Samples were cleaned in an ultrasonic cleaner using isopropanol for 10 minutes and rinsed in distilled water.

The performance of the in-situ fabricated Ti-xPt samples was compared to that of commercially pure Ti (cp-Ti) manufactured via L-PBF using identical process parameters, and to commercially pure Pt (cp-Pt) wire as reference materials.

2.3 Structural analysis: density, micro-hardness and phase composition

Optical microscopy was undertaken using an Olympus GX51 microscope, and Stream Essential software was employed for imaging. Microscopy imaging planes: All optical micrographs presented in this study were captured from the XY-plane (perpendicular to the build direction) to observe the cross-sectional microstructure and Pt particle distribution within the Ti matrix.

Scanning electron microscopy: A Zeiss MERLIN scanning electron microscope (SEM) operated at 15 kV acceleration voltage was used for high-resolution microstructural analysis. EDS analysis: Energy-dispersive X-ray spectroscopy (EDS) analysis was performed using an Oxford Instruments detector integrated with the SEM system. EDS point analyses were conducted at various locations across the Pt-rich particles to quantify elemental composition gradients. The EDS system was calibrated using pure element standards before analysis, and all measurements were performed at 15 kV with a working distance of 8.5 mm to ensure optimal spatial resolution and detection sensitivity.

Density measurements: Archimedes-method density measurements were done to quantify relative density of the built samples. A Kern and Sohn GmbH, model ABT 120-5DM scale was used. The suspension liquid used was isopropanol to reduce the formation of air bubbles on the rough sample surface and thereby achieving more consistent measurements. To calculate the relative density of samples, a theoretical density of 4.507 g/cm^3 and 21.09 g/cm^3 for Ti and Pt were used, respectively [9]. The relative density for each sample was calculated from taking the average of 3 measurements.

X-ray diffraction (XRD) was performed using a Bruker D2 Phaser diffractometer (Cu-Kα source Cu Kα λ = 1.54056 Å) with a standard Bragg Brentano geometry. Voltage of 30 kV and 10 A acquisition dwell time was 0.75 second at steps of 0.01°. Rotation speed was 30 rpm. XRD reference patterns for phase identification were obtained from the Crystallography Open Database (COD) [10]. The lattice parameters were obtained by least squares refinement of data in the 2θ range of 20°–80° with the aid of a Rietveld refinement program MAUD [11].

Micro-hardness testing: Vickers microhardness indentations were conducted according to ASTM standard E348-10 using an Emcotest DuraScan automatic indentation machine. Load

application was 2 kg-force for 10 seconds. A minimum of 10 measurements were made per sample. Sample surface was polished using the steps described in Section 2.1.

2.4 Electrochemical analysis

The electrochemical characterisation was performed ex-situ in a three-electrode glass-cell setup. The counter electrode was a platinum wire, the Ag/AgCl electrode was used as the reference electrode. To accurately report the potential with respect to the reversible hydrogen electrode (RHE), the reference electrode was calibrated for the electrochemical test series by saturating the electrolyte solution with H_2 gas and measuring the open-circuit potential of the reference electrode versus a polycrystalline platinum electrode in the same electrolyte. The Ti-xPt samples were connected as the working electrodes for the electrochemical cell. A 0.5M H2SO4 electrolyte solution was used to conduct the electrochemical measurements.

The prepared electrodes were evaluated for their electrochemical activity via the hydrogen evolution reaction (HER). Electrochemical measurements were performed using a Gamry 1010E potentiostat. The electrochemical cell was first purged with Nitrogen for 15 min before any conditioning or tests were conducted. Cyclic voltammetry (CV) was first used to activate the catalysts and remove contaminants and synthesis residuals from the catalyst surface. The catalysts were cycled between 0.05 – 1.2 V vs the reversible hydrogen electrode (RHE) for 10 cycles at a scan rate of 50 mV/s, followed by a further 10 cycles within the same potential range at a scan rate of 10 mV/s.

Following the conditioning via CV, linear sweep voltammetry (LSV) was performed to evaluate the performance of the electrode. A LSV sweep from 0 – (-0.6) V vs RHE with a scan rate of 10mV/s was done. Open circuit potential was determined by measuring after a 1-minute delay period. Potentiodynamic polarisation was conducted from -0.3 V more negative than the Open Circuit potential (E_{OCP}) to 0.3 V positive of the E_{OCP} at rate of 0.6 mV/s. The sampling frequency was set to 1 s.

3 Results and discussion

3.1 Relative density and micro-hardness

Relative density results of the samples are tabulated in Table 2. The samples with 5wt% Pt exhibited full density which indicates that set A and B process parameters were adequate to achieve full melting. The samples with 10wt% Pt gave lower relative densities of ~91% for both sets A and B process parameter.

Table 2. Relative density of samples

Pt content	Process parameter set	Relative density [%]
5 wt%	A	100.87
	B	100.37
10 wt%	A	91.79
	B	91.63

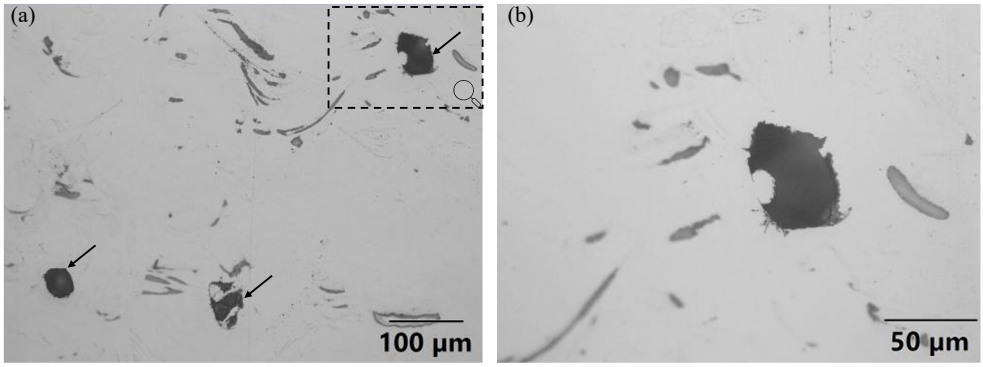

Fig. 1. Micrographs of particle-like vacancies in the 10wt%_A sample.

Analysis of density variations: Optical micrographs of the 10 wt% samples (Figure 1) reveal circular holes on the surface with dimensions on the order of the powder particle size. These holes are likely voids left by Pt particles that were dislodged during grinding and polishing, suggesting that the Pt-Ti interface did not fully melt and fuse during the L-PBF process.

Table 3. Material properties of titanium and platinum [9].

	Ti	**Pt**
Density [g/cm^3]	4.507	21.09
Melting point [°C]	1941	2041
Thermal conductivity [W/m·K]	21.9	71.6
Heat capacity [J/g·K]	0.52	0.13
Heat of fusion [kJ/mol]	15.5	19.6

The observed lack of fusion of the Pt particles is attributed to the significant differences in thermodynamic properties between Ti and Pt, which substantially influence their L-PBF processing behaviour. Key thermodynamic properties are listed in Table 3. Pt, with its higher melting point (2041 K versus 1941 K for Ti) and substantially higher thermal conductivity (71.6 W/m·K versus 21.9 W/m·K), requires greater laser energy input but dissipates heat rapidly, creating challenges in maintaining stable melt pools and increasing risks of incomplete fusion. Conversely, titanium's significantly higher heat capacity (0.52 J/g·K versus 0.13 J/g·K for Pt) means it heats more slowly and maintains temperature more consistently, though its poor thermal conductivity can lead to overheating and problematic thermal gradients.

Microhardness analysis: Fig. **2** plots the measured Vickers hardness values of the cp-Ti, 5wt% and 10wt% Pt samples. The average hardness for cp-Ti sample measured 202.7±7.7 HV2, which matches the typical value obtained in literature [12]. Both process parameter sets A and B achieved similar hardness and were therefore grouped together in the figures. The 5 wt% Pt sample achieved 296±6.8 HV2, and the 10 wt% achieved 325±5.8 HV2.

The increase in Vickers hardness demonstrates that the addition of Pt had a strengthening effect on Ti. Since the indentations were made on the Ti matrix, the increase in hardness indicates that diffusion of Pt into the surrounding material occurred, which agrees with the microstructural analysis presented in the following section.

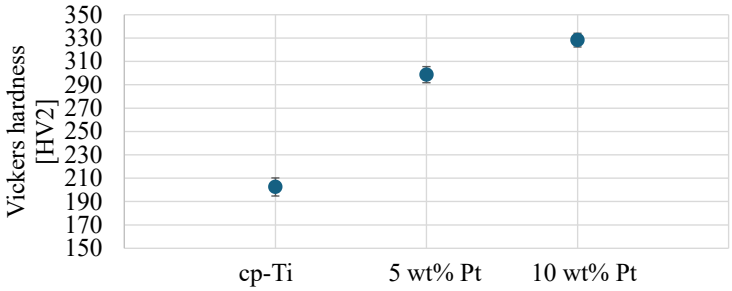

Fig. 2. Vickers hardness of samples

3.2 Phase and microstructure

The optical microscopy revealed that all samples exhibited Pt particles in a matrix of Ti. The boundaries of the Pt particles showed evidence of partial mixing and diffusion into the Ti matrix. No noticeable differences were observed for the samples printed using process parameter set A and B, while the only difference between the 5 wt% and 10 wt% samples was that the latter had a larger number of Pt particles present. The following phase and microstructural characterization of sample 10wt%_B is therefore representative of the microstructural observations of all Ti-xPt samples.

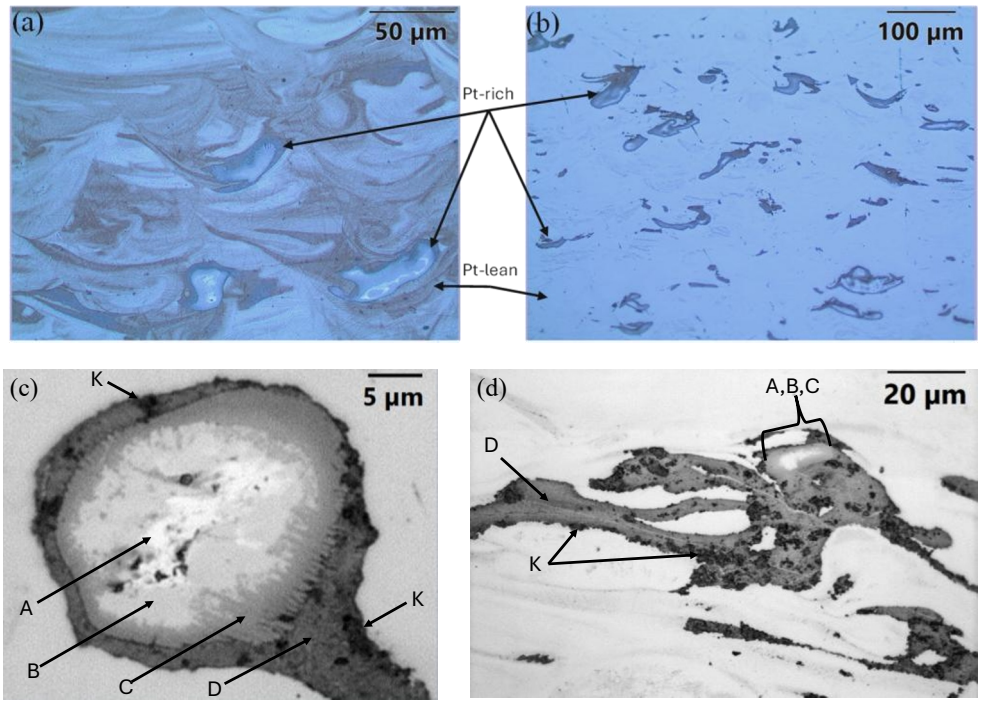

Fig. 3. Optical micrographs showing (a) high magnification before cleaning, (b) low magnification after cleaning (c) high magnification of a Pt-rich particle after cleaning with labels of phases (d) low magnification of Pt-rich zone to show extent of phase K distribution within phase D.

Microstructural observations: Fig. **3**(a) depicts optical micrographs of sample 10wt%_B immediately after etching and displays shades of brown zones surrounding particle-like grey-blue zones. Fig. **3**(b) depicts the same sample, but after cleaning the etched surface with a soft cotton cloth. This had the effect of removing the brown zones leaving only the particle-like zones. From this observation the particles-zones are identified and labelled as Pt-rich zones, the brown-shaded zones the Pt-lean zones. This finding is significant since it provides unmistakable evidence of significant Pt-diffusion in the Ti material, which is not evident from the cleaned surface in Fig. **1** and Fig. **3**(b).

Phase identification within particles: Fig. **3**(c) depict a high magnification of a Pt-rich particle and labels the distinct phases according to their grey-scale shading and texture. Imaging plane clarification: All microstructural images presented were captured from the XY-plane (perpendicular to the build direction) to show the cross-sectional view of the Pt particles and their interaction with the surrounding Ti matrix. Identified phases increase in darkness value form A (brightest) to K (darkest). Fig. **3**(d) depicts a lower magnification image of a large Pt-rich particle with a larger area of phase D compared to phases A-C, which are grouped as single particle. Phase K appears as dark clusters of dark spots dispersed throughout phase D.

Quantitative composition analysis: Figure 4 labels the same phases identified in Figure 3 and tabulates the EDS quantification of their elemental composition. The brightest phase (phase A) measured approximately 100% Pt, while the slightly darker zone (phase B) measured 85.61% Pt. Phase C showed compositional variation, with darker and lighter regions measuring 61.84% and 74.82% Pt, respectively. Phase D measured 48.35% Pt, and the Pt-lean phase outside the boundary of phase D measured 9.12% Pt (similar to the nominal weight percentage of Pt in the sample – 10%).

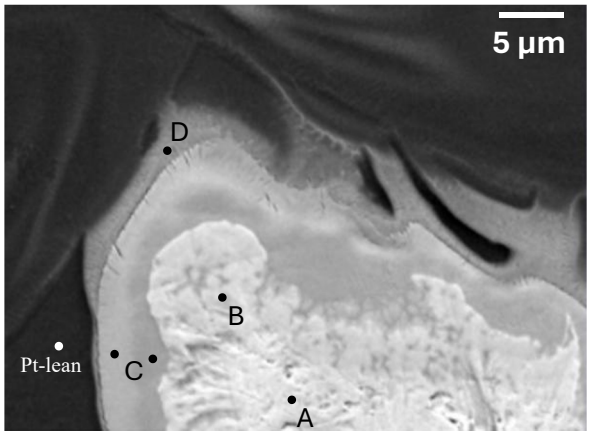

Phase	Pt content [wt%]
A	99.14
B	85.61
C (dark)	61.84
C (light)	74.82
D	48.35
Pt-lean	9.12

Fig. 4. (a) BS-SEM images of Pt-rich particle with identification and labelling of separate regions zone. (b) EDS-SEM point measurement of elemental composition of phases.

3.3 Phase identification

Fig. **5** plots the XRD Bragg peaks patterns for all samples including cp-Ti as the reference. Identified peaks are labelled with their angle, lattice plane and phase icon (of which the corresponding phase is listed in the figure legend). Refinement of peaks identified both the

expected hexagonal close-packed Ti phase (space group P63/mmc, a=2.9410 Å, c=4.6701 Å) and body-centred cubic Ti phase (space group Im-3m, a=3.24368).

Intermetallic phase identification: Low-intensity peaks were more challenging to identify. A peak at 2θ=36.22° was matched with the orthorhombic phase of Ti [13]. Additional low intensity peaks were matched with Ti3Pt in the 10wt%_B sample (cubic symmetry, space group Pm-3n, lattice parameter a=5.031 Å). A single peak at 2θ=29.52° matched that of Ti_2Pt phases (tetragonal symmetry, space group I4/mmm, lattice parameters a=3.18519 Å, c=9.62595 Å).

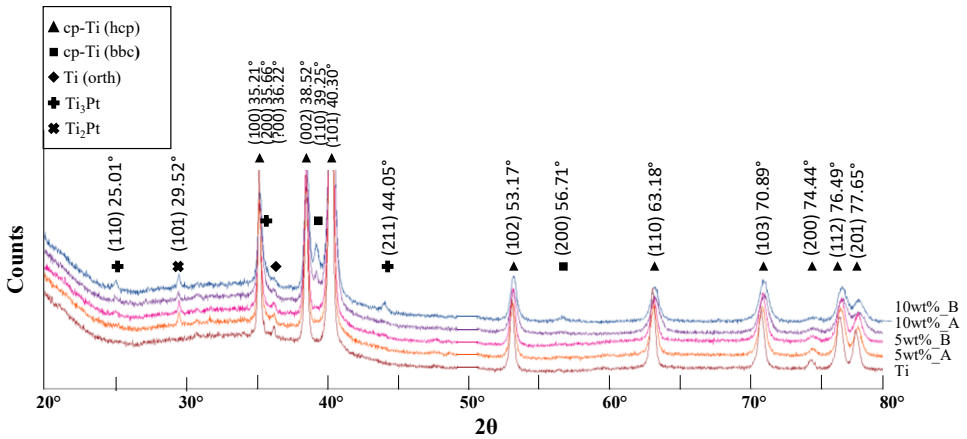

Fig. 5. XRD patterns for samples with patterns and peaks identified.

3.4 Electrochemical behaviour

Corrosion analysis: Figure 6 plots the potentiodynamic polarization curves (Tafel curves) of the Ti-xPt and cp-Ti samples. The corrosion potential (E_{corr}) and corrosion current density (I_{corr}) were determined through Tafel extrapolation analysis of both anodic and cathodic portions of the curves, with results compiled in Table 4. The Ti-xPt samples achieved E_{corr} values in the narrow range of -10.9 to -23.3 mV versus RHE. I_{corr} values fell in a broader range of 11.7 to 155.9 µA/cm².

Compared to the reference cp-Ti sample, which measured a E_{corr} of -304.5 mV, the Ti-xPt samples achieved a significant increase in E_{corr} and therefore an increase in corrosion resistance. This low values suggest that the HER rate determining step is the electrochemical desorption-oriented Volmer–Heyrovsky mechanism [14].

Passivation behaviour: When the potential increased above E_{corr}, the current remained approximately constant, indicating that the system operates under "passivation control" rather than "activation control" in the anodic region. This means the rate-determining step is related to passive film formation and maintenance rather than simple charge transfer kinetics. The Pt particles likely created galvanic coupling with titanium regions, promoting the formation of protective oxide films.

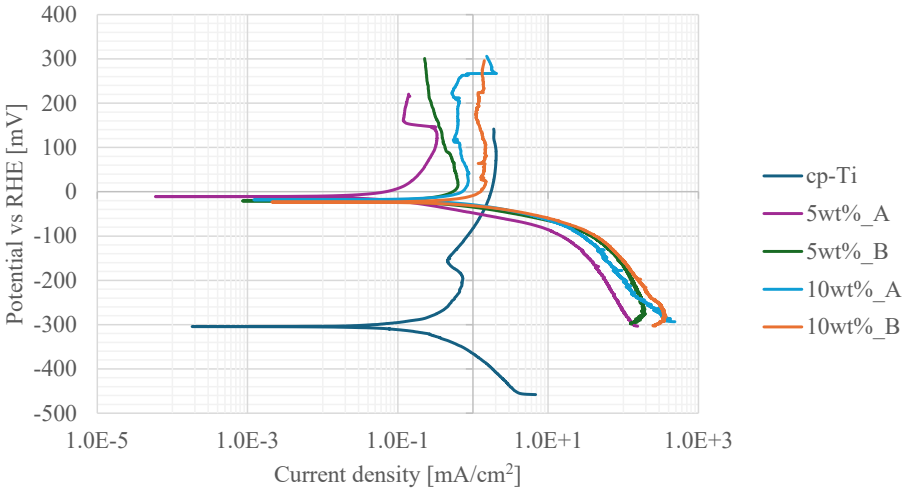

Fig. 6. Electrochemical characteristics of the cp-Ti and the 5 and 10 wt% Pt samples of process parameters sets A and B.

Table 4. Quantified corrosion potentials, corrosion current densities and Tafel slope gradients from the plotted Tafel curves.

Sample	E_{corr} versus RHE [mV]	I_{corr} [µA/cm^2]	Tafel slope [mV·dec^{-1}]
cp-Ti	-304.5	59.8	168.40
5wt%_A	-10.9	11.7	40.53
5wt%_B	-20.7	79.2	40.03
10wt%_A	-18.2	136.3	52.02
10wt%_B	-23.3	155.9	40.54

Mechanism of improved corrosion resistance: The positive shift in E_{corr} indicates the beneficial influence of Pt on the corrosion resistance of cp-Ti. This improvement is attributed to the promotion of the active-passive transition by enhanced cathodic reactions. Due to the lower electronegativity of Ti (1.54) compared to Pt (2.28), electrons migrate toward Pt atoms in the alloy. The addition of Pt promotes oxygen reduction at cathodic areas around the Pt atoms, and the enhanced cathodic reaction accelerates spontaneous passivation of the Ti surface at anodic areas.

HER performance evaluation: Polarization curves for Ti-xPt, cp-Ti, and cp-Pt samples are plotted in Figure 7. The noise in the data resulted from H_2 bubble formation on the electrode surface. As expected, the reference cp-Ti showed no significant HER activity in the investigated potential range. The Ti-xPt samples all demonstrated similar or improved HER activity compared to cp-Pt, with the 5wt%_A sample achieving comparable HER activity to cp-Pt. All samples displayed similar HER onset potentials of approximately 25-30 mV.

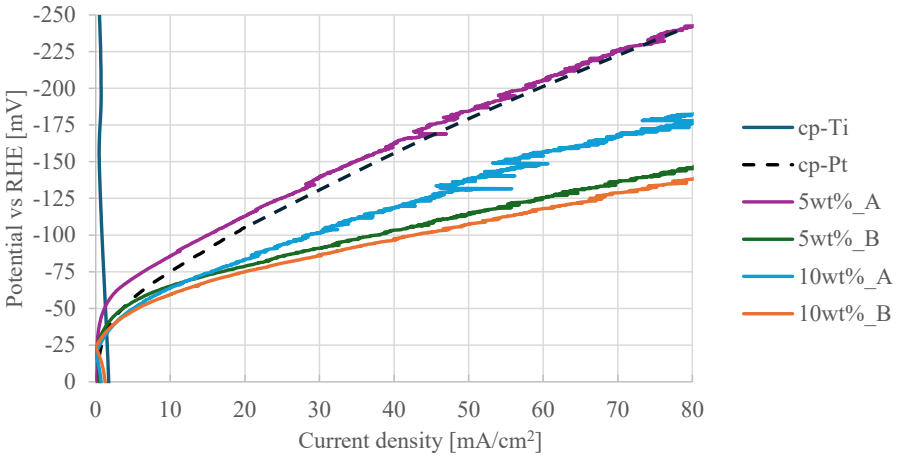

Fig. 7. Polarisation curves of all samples.

Overpotential comparison: The overpotential at 10 mA/cm² versus RHE (Table 5) serves as a benchmark for comparing HER performance with literature studies. These values indicated that all Ti-xPt samples except 5wt%_A recorded improved overpotentials compared to cp-Pt, meaning these samples require lower energy input to generate equivalent amounts of H_2 gas. When compared to Pt polarization curves reported by Swaminathan *et al.* [14], the current study measured nearly identical cp-Pt overpotential values at 10 mA/cm² versus RHE (-75 mV), validating the reliability of the experimental setup and results.

Table 5. Overpotentials of samples at 10 mA/cm^2.

Sample	Overpotential at 10 mA/cm^2 (vs RHE) [mV]
cp-Pt	-75.0
5wt%_A	-85.8
5wt%_B	-65.3
10wt%_A	-64.0
10wt%_B	-59.4

Performance implications and cost benefits: The results are very encouraging since they suggest by using *in-situ* L-PBF of 5wt% Pt combined with 95 wt% Ti, an improved HER performance to cp-Pt can be achieved. This has significant cost saving benefits since only a small amount of Pt is required to generate similar-to-improved HER activity.

Mechanistic discussion: The following briefly discusses possible reasons for the improved performance. A study by Komatsu *et al.* [15] found that intermetallic compounds such as Ti_3Pt and $TiPt_3$ measure an higher HER activity than pure Pt. Since the presence of Ti_3Pt was observed in the XRD plots, this is the strongest evidence-based theory for the improvement observed. Another aspect that might have contributed to the improved performance of the Ti-xPt samples is the fine dispersion of the Pt particles over the electrode surface, Fig. **3**(b). This might have improved the bubble nucleation dynamics during hydrogen evolution.

Future characterization needs: To provide a conclusive mechanistic explanation for the improved HER performance of the Ti-xPt samples requires repeating the experiments and conducting additional analysis of their electrochemical behaviour. Future analysis will therefore incorporate DC resistivity measurements, electrochemical impedance

spectroscopy, and Mott-Schottky analysis to better understand the underlying mechanisms responsible for the enhanced electrochemical performance.

4 Conclusion

This study successfully demonstrated the feasibility of in-situ alloying of Ti-xPt (x = 5, 10 wt%) using L-PBF technology. The research provides valuable insights into both the processing challenges and performance benefits of these novel alloys. Several significant conclusions can be drawn from this investigation:

First, the L-PBF process parameters significantly influenced the quality of the produced Ti-xPt alloys. While the 5 wt% Pt samples achieved full density (>100%) with both parameter sets, the 10 wt% samples exhibited lower relative density (~91%) due to incomplete fusion at the Ti-Pt interfaces. This finding highlights the critical impact of the thermodynamic property differences between Ti and Pt, particularly the higher melting point and thermal conductivity of Pt compared to Ti.

Microstructural analysis revealed complex phase formations at the Ti-Pt interfaces. The presence of Ti_3Pt and Ti_2Pt intermetallic compounds was confirmed through XRD analysis, demonstrating that despite incomplete homogenization, significant diffusion and reaction occurred between the constituent materials. This partial alloying was further evidenced by the increase in Vickers hardness from 202.7±7.7 HV2 for cp-Ti to 296±6.8 HV2 and 325±5.8 HV2 for 5 wt% and 10 wt% Pt samples, respectively.

The electrochemical evaluation yielded particularly promising results. The Ti-xPt samples demonstrated significantly improved corrosion resistance compared to cp-Ti, with E_{corr} shifting positively from -304.5 mV for cp-Ti to between -10.9 and -23.3 mV for the Ti-xPt samples. Most notably, the hydrogen evolution reaction (HER) performance of the Ti-xPt alloys was equal to or better than pure platinum, with most samples requiring lower over-potentials at 10 mA/cm² than cp-Pt. The 10 wt%_B sample achieved the lowest over-potential of -59.4 mV, compared to -75.0 mV for cp-Pt.

These results have significant implications for both manufacturing and application domains. From a manufacturing perspective, this study demonstrates that L-PBF can effectively process Ti-Pt alloys with minimal platinum content, addressing the cost and resource efficiency challenges associated with platinum-based materials. From an applications standpoint, the enhanced corrosion resistance and superior HER performance position these alloys as promising candidates for biomedical implants and energy conversion devices, particularly water electrolysis systems.

Future work should focus on optimizing process parameters through a systematic design of experiments approach to achieve full density in higher Pt-content samples. Additionally, investigating the lower threshold of Pt content necessary for improved electrochemical performance could further enhance cost-effectiveness. To fully understand the mechanisms behind the improved HER activity, more comprehensive electrochemical characterization including DC resistivity measurements, electrochemical impedance spectroscopy, and Mott-Schottky analysis is recommended.

In conclusion, this study not only advances the fundamental understanding of the Ti-Pt system but also demonstrates the potential of L-PBF as both a manufacturing method for

these high-value alloys and as an investigative tool for exploring complex intermetallic systems with promising functional properties.

This research was funded by the South African Department of Science, Technology and Innovation through the CSIR for the Collaborative Program in Additive Manufacturing (Contract No. CSIR-NLC-CPAM-21_MOA-CUT-01).

References

[1] T.C. Dzogbewu, Additive manufacturing of TiAl-based alloys, Manuf. Rev. 7 (2020) 35. doi:10.1051/mfreview/2020032.

[2] U. Arshad, J. Tang, Z. Shao, Replace Platinum for Hydrogen Evolution Reaction in the Cathode of Proton Exchange Membrane Water Electrolyzers, SusMat. 5 (2025). doi:10.1002/sus2.267.

[3] M. Sarraf, E. Rezvani Ghomi, S. Alipour, S. Ramakrishna, N. Liana Sukiman, A state-of-the-art review of the fabrication and characteristics of titanium and its alloys for biomedical applications, Bio-Design Manuf. 5 (2022) 371–395. doi:10.1007/s42242-021-00170-3.

[4] N. Dubouis, A. Grimaud, The hydrogen evolution reaction: from material to interfacial descriptors, Chem. Sci. 10 (2019) 9165–9181. doi:10.1039/C9SC03831K.

[5] M.F. Lagadec, A. Grimaud, Water electrolysers with closed and open electrochemical systems, Nat. Mater. 19 (2020) 1140–1150. doi:10.1038/s41563-020-0788-3.

[6] S. Chowdhury, N. Yadaiah, C. Prakash, S. Ramakrishna, S. Dixit, L.R. Gupta, D. Buddhi, Laser powder bed fusion: a state-of-the-art review of the technology, materials, properties & defects, and numerical modelling, J. Mater. Res. Technol. 20 (2022) 2109–2172. doi:10.1016/j.jmrt.2022.07.121.

[7] H.-J. Song, M.-K. Han, H.-G. Jeong, Y.-T. Lee, Y.-J. Park, Microstructure Analysis of Ti-xPt Alloys and the Effect of Pt Content on the Mechanical Properties and Corrosion Behavior of Ti Alloys, Materials (Basel). 7 (2014) 3990–4000. doi:10.3390/ma7053990.

[8] F. Bartolomeu, M. Gasik, F.S. Silva, G. Miranda, Mechanical Properties of Ti6Al4V Fabricated by Laser Powder Bed Fusion: A Review Focused on the Processing and Microstructural Parameters Influence on the Final Properties, Metals (Basel). 12 (2022) 986. doi:10.3390/met12060986.

[9] Author, Platinum – Melting Point – Boiling Point, (2021). https://www.nuclear-power.com/platinum-melting-point-boiling-point/.

[10] Crystallography Open Database, (n.d.). https://www.crystallography.net/cod/.

[11] L. Lutterotti, Total pattern fitting for the combined size–strain–stress–texture

determination in thin film diffraction, Nucl. Instruments Methods Phys. Res. Sect. B Beam Interact. with Mater. Atoms. 268 (2010) 334–340. doi:10.1016/j.nimb.2009.09.053.

[12] S.S. da Rocha, G.L. Adabo, G.E.P. Henriques, M.A. de A. Nóbilo, Vickers hardness of cast commercially pure titanium and Ti-6Al-4V alloy submitted to heat treatments, Braz. Dent. J. 17 (2006) 126–129. doi:10.1590/S0103-64402006000200008.

[13] G.M. Ter Haar, T.H. Becker, Laser powder bed fusion produced Ti-6Al-4V: Influence of high-energy process parameters on in-situ martensite decomposition and prior beta grain texture, J. Alloys Compd. 918 (2022) 165497. doi:10.1016/j.jallcom.2022.165497.

[14] J. Swaminathan, R. Subbiah, V. Singaram, Defect-Rich Metallic Titania (TiO 1.23)—An Efficient Hydrogen Evolution Catalyst for Electrochemical Water Splitting, ACS Catal. 6 (2016) 2222–2229. doi:10.1021/acscatal.5b02614.

[15] T. Komatsu, D. Satoh, A. Onda, Ti–Pt intermetallic compound catalysts more active than Pt for hydrogen dissociation and ethylene hydrogenation, Chem. Commun. (2001) 1080–1081. doi:10.1039/b102415a.